NJC

Molecular structure, optical and magnetic properties of free-base tetrapyrazinoporphyrazine in various reduction states

Journal:	*New Journal of Chemistry*
Manuscript ID	NJ-ART-09-2019-004775.R1
Article Type:	Paper
Date Submitted by the Author:	08-Nov-2019

Complete List of Authors:	Konarev, Dmitri; Institute of Problems of Chemical Physics RAS, Faraonov, Maxim; Institute of Problems of Chemical Physics of RAS, ; Institute of Problems of Chemical Physics Kuz`min, Alexey; Institute of Solid State Physics RAS, Osipov, Nikita; Institute of Problems of Chemical Physics of RAS Khasanov, Salavat; Institute of Solid State Physics RAS, Otsuka, Akihiro; Research Center for Low Temperature and Materials Sciences, Kyoto University, Sakyo-ku, 606-8501, Yamochi, Hideki; Kyoto University, Kitagawa, Hiroshi; Kyoto University, Department of Chemistry Lyubovskaya, Rimma; Institute of Problems of Chemical Physics RAS,

ARTICLE

Received 00th January 20xx,

Accepted 00th January 20xx

DOI: 10.1039/x0xx00000x

Molecular structure, optical and magnetic properties of free-base tetrapyrazinoporphyrazine in various reduction states

Dmitri V. Konarev [*a] Maxim A. Faraonov,[*a] Alexey V. Kuzmin,[b] Nikita G. Osipov, [a, c] Salavat S. Khasanov, [b] Akihiro Otsuka,[d, e] Hideki Yamochi,[d, e] Hiroshi Kitagawa [d] Rimma N. Lyubovskaya [a]

Reduction of free-base tetrapyrazinoporphyrazine (H_2TPyzPz) in different experimental conditions allowed us to obtain radical anion salt {cryptand[2.2.2](K^+)}$_2$(H_2TPyzPz$^{\bullet-}$)$_2$·3$C_6H_4Cl_2$ (**1**), and dianion salts {cryptand[2.2.2](K^+)}$_2$(H_2TPyzPz^{2-})·$C_6H_4Cl_2$ (**2**) and {cryptand[2.2.2](K^+)}$_2$(H_2TPyzPz^{2-})·[CpFe(CO)$_2$]$_2$·3$C_6H_4Cl_2$ (**3**) in the form of single crystals. Molecular structure, optical and magnetic properties of free-base tetrapyrazinoporphyrazine in various reduction states were studied for the first time. Reduction of the macrocycle is accompanied by the appearance of alternation of the C-N_{meso} bonds, blue shift of both Soret and Q-bands as well as the appearance of new bands in the NIR range. Salt **1** contained paramagnetic H_2TPyzPz$^{\bullet-}$ radical anions half of which formed face-to-face type dimers with very effective π-π interaction, whereas the rest ones were magnetically isolated from other H_2TPyzPz$^{\bullet-}$ radical anions. Strong antiferromagnetic coupling of spins with a magnetic exchange interaction of J/k_B = -140 K was observed in these dimers. In **2** and **3**, diamagnetic dianions H_2TPyzPz^{2-} were completely isolated.

Introduction

Phthalocyanines (Pcs) and their metal complexes are generally used as dyes, catalysts, materials for optical, electronic and photoelectronic devices as well as sensitizers in photodynamic tumor therapy [1-5]. At one reduction or oxidation of these macrocycles, the generated unpaired electron can be either delocalized over the macrocycle or localized on the central metal atom. This electron can provide high conductivity or magnetic ordering of spins. Oxidation chemistry of Pcs has being developed for a long time. Highly conducting compounds and complexes with magnetic ordering of spins based on oxidized metal phthalocyanines or related macrocycles were obtained [6-9]. In last years it was also shown that reduced Pcs can be interesting objects to develop functional compounds [10-26]. To reduce Pcs, strong reductants such as zinc dust [12, 13], Na/Hg [14], potassium graphite (KC_8) [15, 16], LiCp* [17], decamethylchromocene [11, 18], and sodium fluorenone ketyl [19-26] were applied.

Tetrapyrazinoporphyrazines (TPyzPzs) are aza analogs of phthalocyanine with stronger acceptor properties due to the presence of four acceptor pyrazine fragments instead of phenylene groups [27-30]. The 1st reduction potentials of the TPyzPz derivatives (– 0.4 to – 0.6 V vs SCE) are more positive by 0.2–0.4 V compared with those for the corresponding Pc compounds (– 0.7 to – 0.9 V vs SCE) [30]. Due to redox potentials of TPyzPzs are essentially more positive in comparison with those of Pcs[27-30], they can have more air stable radical anion and dianion forms. Only several anionic compounds with the TPyzPz macrocycles are known at present [31-34] which were obtained by using sodium fluorenone ketyl [31-33] or zinc dust [34] as reductant. For example, the diamagnetic salt with the H_2TPyzPz^{2-} dianions was obtained by the reduction of free-base tetrapyrazinoporphyrazine by sodium fluorenone ketyl in the presence of cryptand[2.2.2] [31].

In this work we report on the reduction of free-base tetrapyrazinoporphyrazine in different experimental conditions. The reduction yielded the first radical anion salt of this macrocycle {cryptand[2.2.2](K^+)}$_2$(H_2TPyzPz$^{\bullet-}$)$_2$·3$C_6H_4Cl_2$ (**1**) besides additionally to the dianion salts {cryptand[2.2.2](K^+)}$_2$(H_2TPyzPz^{2-})·$C_6H_4Cl_2$ (**2**) and {cryptand[2.2.2](K^+)}$_2$(H_2TPyzPz^{2-})·[CpFe(CO)$_2$]$_2$·3$C_6H_4Cl_2$ (**3**) as single crystals. These salts were used by us for the first time to study free-base tetrapyrazinoporphyrazine in various reduction states comparing their molecular structure, optical and magnetic properties. As a result, it is obvious that reduction provides the appearance of alternation of C-N_{meso} bonds, the blue shift of both Soret and Q-bands and the appearance of new bands in the NIR range.

[a] *Institute of Problems of Chemical Physics RAS, Chernogolovka, Moscow region, 142432 Russia;. E-mail: konarev3@yandex.ru, maksimfaraonov@yandex.ru*
[b] *Institute of Solid State Physics RAS, Chernogolovka, Moscow region, 142432 Russia;*
[c] *Moscow State University, Leninskie Gory,119991 Moscow, Russia;*
[d] *Division of Chemistry, Graduate School of Science, Kyoto University, Sakyo-ku, Kyoto 606-8502, Japan;*
[e] *Research Center for Low Temperature and Materials Sciences, Kyoto University, Sakyo-ku, Kyoto 606-8501, Japan.*

† Electronic supplementary information (ESI) available: The IR spectra of the starting compounds and salts **1–3**. Data of EPR measurements of salts **1**-**3**. CCDC 1952192, 1952193 and 1952194. See DOI: 10.1039/x0xx00000x

Results and discussion

Synthesis

Previously, H_2TPyzPz and $Ti^{IV}O$(AceTPyzPz) (AceTPyzPz - tetra(acenaphthenopyrazino)porphyrazine) were successfully reduced by sodium fluorenone ketyl (E_{redox} = –1.3 V *vs* SCE [35]) in the presence of cryptand[2.2.2] or PPNCl (PPN^+ is bis(triphenylphosphoranylidene)ammonium cation), and dianionic $H_2TPyzPz^{2-}$ [31] or tetraanionic $AceTPyzPz^{4-}$ macrocycle were formed in $\{Ti^{IV}O(AceTPyzPz)^{4-}\}^{2-}$ [32]. Zinc dust is also a suitable reductant (E_{redox} = –0.762 V *vs* SHE [36]) for the preparation of anionic salt of iron(II) octaethyltetrapyrazinoporphyrazine. In this case, the macrocycle is reduced to dianion state by the aid of additional $ZnCl_2$ which coordinated to the periphery of macrocycle to enhance the acceptor property [34].

Strong reductant potassium graphite (KC_8) can produce radical anion and dianion forms of H_2TPyzPz. In this case the degree of reduction is controlled by the amount of cryptand[2.2.2.] which is a source of{cryptand[2.2.2](K^+)} cations. KC_8 is completely insoluble in *o*-dichlorobenzene without cryptand[2.2.2.]. Reduction of H_2TPyzPz in the presence of one equivalent of cryptand[2.2.2] leads to the formation of deep blue radical anion salt $\{cryptand[2.2.2](K^+)\}_2(H_2TPyzPz^{\bullet-})_2{\cdot}3C_6H_4Cl_2$ (**1**) whose composition was determined from X-ray diffraction on single crystals.

The use of two equivalents of cryptand[2.2.2] with an excess of KC_8 allows a deep violet dianion salt of H_2TPyzPz to be generated. To improve crystal growth we added the excess of well soluble metalloorganic compound cyclopentadienyliron dicarbonyl dimer ($[CpFe(CO)_2]_2$) during the synthesis. Generally, these dimers improve crystal growth of anionic macrocyclic salts without incorporation into the crystals [20]. However, in this case the $[CpFe(CO)_2]_2$ dimers are incorporated into the crystals to form $\{cryptand[2.2.2](K^+)\}_2(H_2TPyzPz^{2-}){\cdot}[CpFe(CO)_2]_2 \cdot 3C_6H_4Cl_2$ (**3**) salt containing $H_2TPyzPz^{2-}$ dianions whose composition was determined from X-ray diffraction on single crystals.

We also studied the interaction of the $H_2TPyzPz^{\bullet-}$ radical anions with vanadocene (Cp_2V^{II}) which potentially can coordinate to the periphery of the TPyzPz macrocycle containing three outer nitrogen atoms. However, the addition of two equivalents of vanadocene to the solution of salt **1** resulted in further reduction of $H_2TPyzPz^{\bullet-}$ to $H_2TPyzPz^{2-}$ and the formation of deep violet solution characteristic of $H_2TPyzPz^{2-}$ (similar color of the solution was observed at the synthesis of **3**). Slow mixing of the obtained solution with *n*-hexane yielded $\{cryptand[2.2.2](K^+)\}_2(H_2TPyzPz^{2-}){\cdot}C_6H_4Cl_2$ (**2**) salt whose composition was also determined by X-ray diffraction on single crystals. This salt contains smaller number of $C_6H_4Cl_2$ molecules in comparison with the dianion salt $\{cryptand[2.2.2](Na^+)\}_2(H_2TPyzPz^{2-}){\cdot}2C_6H_4Cl_2$ (**4**) published previously [31]. It is also seen that vanadocene or vanadocene cations are not incorporated into the crystals formed. Probably $\{cryptand[2.2.2](K^+)\}$ cations form more stable structure in comparison with the vanadocenium cations. It should also be mentioned that the usage of slightly larger $\{cryptand[2.2.2](K^+)\}$ ion instead of $\{cryptand[2.2.2](Na^+)\}$ ion provided the formation of the salt with smaller number of solvent molecules and completely different crystal structure.

It should be noted that the reduction of free-base phthalocyanine by an excess of KC_8 in the presence of two equivalents of cryptand[2.2.2] gives no dianion salt corresponding to weaker acceptor properties of H_2Pc in comparison with that of H_2TPyzPz. Previously, similar behavior was found at the electrochemical reduction of these free-base macrocycles [37].

Optical properties

Reduction of tetrapyrazinoporphyrazine macrocycle accompanied by the formation of the $H_2TPyzPz^{\bullet-}$ radical anions in **1** and $H_2TPyzPz^{2-}$ dianions in **2** and **3** affects optical properties of the macrocycles. IR spectra of starting compounds and salts **1-3** measured in KBr pellets are shown in Fig. S1, and absorption bands are listed in Table S1. IR spectra of **1-3** are a superposition of those for pristine H_2TPyzPz, cryptand[2.2.2] and solvent molecules (Fig. S1, Table S1). IR spectrum of **3** additionally contains absorption bands attributed to $[CpFe(CO)_2]_2$. Some absorption bands of H_2TPyzPz are essentially shifted or change in intensity at the formation of the salts (Table S1). For example, the strong band at 891 cm^{-1} in the spectrum of parent macrocycle is slightly shifted to 890 cm^{-1} in **1** and distinctly moved to 882 cm^{-1} in the spectra of **2** and **3** with the obvious decrease of intensity in all cases. Shift of strong band at 1364 cm^{-1} to smaller wavenumbers is observed in the spectra of salts **1**- **3**. These bands are positioned at 1358, 1354 and 1355 cm^{-1}, respectively. It should be noted that shift of some absorption bands correlates with negative charge on the macrocycle. For example, pristine H_2TPyzPz has two hydrogens atoms bonded to pyrrole nitrogen ones. Previously, it was shown that the formation of $H_2TPyzPz^{2-}$ dianions in **4** [31] and $H_2Pc^{\bullet-}$ [19] is accompanied by shortening of the N–H bonds. The band attributed to the N–H bond vibrations is observed at 3286 cm^{-1} in the spectrum of neutral H_2TPyzPz and is shifted to larger wavenumbers by 16 cm^{-1} in the spectrum of **1** and by 50-51 cm^{-1} in those of **2** and **3**. Thus, reduction of H_2TPyzPz to $H_2TPyzPz^{\bullet-}$ and finally to $H_2TPyzPz^{2-}$ according to the IR data leads to step-by-step shortening of the N–H bonds in the center of the macrocycle.

Spectra of pristine H_2TPyzPz and salts **1-3** in KBr pellets in the UV-visible-NIR range are shown in Fig. 1, and the positions of the absorption bands are listed in Table 1. Pristine H_2TPyzPz shows the Soret band at 336 nm and the Q-band at 644 nm. The formation of salts **1- 3** is accompanied by strong blue shift of both Soret and Q bands as compared with the spectrum of pristine H_2TPyzPz (Table 1). Q-band maximum is shifted by 58 nm at the formation of $H_2TPyzPz^{\bullet-}$ in **1**. At that, two-electron reduction of H_2TPyzPz yields the $H_2TPyzPz^{2-}$ dianions in **2** and **3** and leads to a larger shift of Q-band maximum by 98 nm. Shift of the Soret bands at the reduction of H_2TPyzPz is also more pronounced for $H_2TPyzPz^{2-}$ as compared with $H_2TPyzPz^{\bullet-}$ (Fig. 1). Previously, it was also shown that blue shift of both Soret and Q-bands increases together with negative charge on the macrocycles in the salts of titanyl and vanadyl phthalocyanines [23]. Thus, the increase in negative charge on tetrapyrazinoporphyrazine macrocycle is accompanied by blue shift of the Soret and Q-bands, and this shift is essentially larger for dianions in comparison with the radical anions.

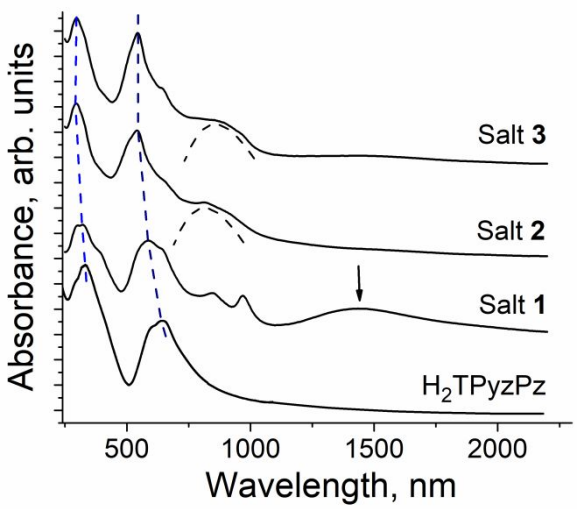

Figure 1. UV-visible-NIR spectra of pristine $H_2TPyzPz$ and salts **1-3** in KBr pellets prepared for **1-3** in anaerobic conditions.

Unlike pristine $H_2TPyzPz$, the spectra of salts **1**-**3** show strong absorption in the NIR range. The $H_2TPyzPz^{\bullet-}$ radical anions show a split absorption band with maxima at 844 and 969 nm, whereas the $H_2TPyzPz^{2-}$ dianions manifest an broad absorption band with maximum at 820 nm in the spectrum of **2** and 860 nm in the spectrum of **3**. Spectrum of previously described salt **4** with the $H_2TPyzPz^{2-}$ dianions has a similar band at 822 nm [31]. Thus, both radical anions and dianions of $H_2TPyzPz$ show characteristic absorption bands in the NIR range allowing these anions to be distinguished by optical spectra.

Table 1. Data of UV-visible-NIR spectra of pristine free-base tetrapyrazinoporphyrazine and salts based on reduced H2TPyzPz.

Compound	Charge state of $H_2TPyzPz$	Position of the absorption bands of $H_2TPyzPz$		
		Soret band, nm	Q-band, nm	Bands in NIR, nm
$H_2TPyzPz$	0	336	607, 644 (max)	-
Salt **1**	−1	314	586 (max), 640	844, 969, 1440 (CT)
Salt **2**	−2	296	546 (max), 626	820
Salt **3**	−2	301	546 (max), 644	860
Salt **4**	−2	296	542 (max), 646	822

An intense broad absorption band is observed in the spectrum of **1** with maximum at about 1440 nm (Fig. 1). This band can be attributed to charge transfer between two $H_2TPyzPz^{\bullet-}$ in the dimers (for description of these dimers see Crystal structures section). Previously it was shown that such bands can appear in optical spectra of the salts containing π-π stacking dimers when macrocycles have very effective π-π interaction. Generally, the formation of π-π stacking dimers provides very effective magnetic coupling between paramagnetic macrocycles in the dimers [22]. Bands in the far-NIR range are not observed in the spectrum of **2** and are very weak in the spectrum of **3** (Fig. 1) indicating only weak π-π interaction between macrocycles in these salts.

Crystal structures of 1-3

Crystal structure of salt **1** contains one whole and two halves of independent of $H_2TPyzPz^{\bullet-}$ radical anion, two independent cryptand[2.2.2](Na^+) cations and solvent *o*-$C_6H_4Cl_2$ molecules. The structures of salts **2** and **3** contain two halves of independent of $H_2TPyzPz^{2-}$, two independent cryptand[2.2.2](Na^+) cations and solvent *o*-$C_6H_4Cl_2$ molecules. The structure of salt **3** additionally contains one molecule of cyclopentadienyliron dicarbonyl dimer ($[CpFe(CO)_2]_2$).

In one of three $H_2TPyzPz$ macrocycles in **1**, the hydrogen atoms in the center of macrocycle show statistic disorder at two sets of positions. As a result, we exclude this molecule from the consideration of bond length in the macrocycle. Two other $H_2TPyzPz^{\bullet-}$ radical anions in **1** and both independent $H_2TPyzPz^{\bullet 2-}$ dianions in **2** and **3** are ordered and are subjected to the discussion of geometry (Table 2).

Table 2. Geometric parameters for phthalocyanine and tetrapyrazinoporphyrazine macrocycles in different compounds and according to DFT calculations.

Compound	Charge state	Average length of the bonds, Å	
		$C\text{-}N_{pyr}$	$C\text{-}N_{meso}$ short/long, difference
Pristine H_2Pc [40]	0	1.372(4)	1.327(2)
$(Bu_4N^+)_2(H_2Pc^{\bullet-})(Br^-)$ [19]	−1	1.375(9)	1.303(8)/1.363(8), 0.060
$(Pr_4N^+)_2(H_2Pc^{\bullet-})(Br^-)$ [19]	−1	1.381(3)	1.309(3)/1.367(3), 0.058
Salt **1** for two of three independent macrocycles	−1	1.367(3) 1.365(3)	1.324(3)/1.335(3), 0.011 1.325(3)/1.334(3), 0.009
Salt **2**	−2	1.382(4) 1.385(4)	1.291(4)/1.378(4), 0.087 1.290(4)/1.382(4), 0.092
Salt **3**	−2	1.385(2) 1.382(3)	1.289(2)/1.374(2), 0.085 1.297(3)/1.371(3), 0.074
Salt **4** [31]	−2	1.384(2)	1.284(2)/1.376(2), 0.092
$H_2TPyzPz$ (DFT) [31]	0	1.380	1.318/1.336, 0.018
$H_2TPyzPz^{\bullet-}$ (DFT) [31]	−1	1.384	1.325/1.338, 0.013
$H_2TPyzPz^{2-}$ (DFT) [31]	−2	1.391	1.303/1.367, 0.064

Neutral phthalocyanine and tetrapyrazinoporphyrazine macrocycles have stable aromatic 18 π-electron systems. Transition to less stable 19 and 20 π-electron systems at the formation of radical anion and dianion macrocycles is accompanied by modulation of some bond lengths in the macrocycles due to alternation of the bonds. There are shorter bonds with *meso*-nitrogen (N_{meso}) atoms and longer bonds with pyrrole (N_{pyr}) nitrogen atoms (Figure 2, Table 2, S2). The crystal structure of pristine tetrapyrazinoporphyrazine is unknown. However, no alteration of these bonds is observed in neutral substituted metal tetrapyrazinoporphyrazines and free-base phthalocyanine [38, 39]. The average difference of 0.009-0.011 Å between short and long C-N_{meso} bonds in the $H_2TPyzPz^{\bullet-}$ radical anions in **1** is essentially smaller in comparison with the $H_2Pc^{\bullet-}$ radical anions (0.058-0.060 Å) [19]. Two-electron reduction of $H_2TPyzPz$ in **2** and **3** leads to essentially stronger alternation of the bonds since average differences between short and long C-N_{meso} bonds are 0.074-0.092 Å in these salts (Table 2). Similar difference was observed in **4** [31] (Table 2). DFT calculations support the observed tendency [31]. In all cases alternation occurs in such a way that short and long C–N_{meso} bonds belong to two oppositely located pyrrolopyrazine units (Figure 2). Thus, reduction of the $H_2TPyzPz$ macrocycle to the radical anion and dianion state leads to the increase of distortion of the macrocycle and provides partial loss of its aromaticity. Such affect is also characteristic of the reduction of phthalocyanine macrocycle [19]. For example, two times larger distortion of the macrocycle is observed for tetraanion Pc^{4-} macrocycle in $[M^{IV}O(Pc^{4-})]^{2-}$(M = Ti, V) in comparison with the radical trianion $Pc^{\bullet 3-}$ macrocycle in $[M^{IV}O(Pc^{\bullet 3-})]^{\bullet-}$) (M = Ti, V) [23]. TPyzPz macrocycle has pyrrole (the N_{pyr} atom with hydrogen) and pyrrolenine (the N_{pyr} atoms without hydrogen) rings. The average length of the C-N_{pyr} bonds as well as the C-N_{pyr}-C angles in the pyrrole rings is larger in comparison with those in the pyrrolenine rings and increases with negative charge on the macrocycle (Table S2). For example, difference between the length of the C-N_{pyr} bonds in the pyrrole and pyrrolenine rinds of $H_2TPyzPz^{\bullet-}$ is within the experimental error. Whereas, this difference (up to 0.028 Å) is in several times larger for the $H_2TPyzPz^{2-}$ dianions. This tendency is supported by DFT calculations (Table S2).

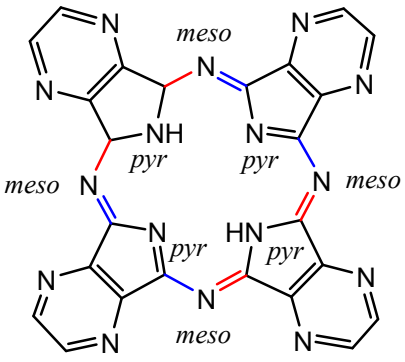

Figure 2. Molecular structure of the $H_2TPyzPz$ macrocycle in radical anions and dianion states. Elongated and shortened C–N_{meso} bonds are shown by blue and red color, respectively.

All $H_2TPyzPz$ macrocycles have almost flat conformation in **1 – 3** with only slight deviation of pyrazine rings from the 24-atom porphyrazine plane.

The crystal structure of salt **1** has two types of the $H_2TPyzPz^{\bullet-}$ radical anions (Fig. 3). Macrocycles of the first type form π–π stacking dimers with interplanar distances of 3.246 Å and multiple short van der Waals (vdW) C,N···C,N contacts between $H_2TPyzPz^{\bullet-}$ in the 3.173 – 3.398 Å range (Fig. 4a). Short interplanar distance in the dimer indicates effective π–π interaction between the macrocycles in **1** and explains the appearance of a charge transfer (CT) band in its NIR spectrum. Macrocycles in the dimer are shifted relative to each other in such way that nitrogen N_{pyr} atoms of one macrocycle are located nearly above the N_{pyr} atoms of the neighbouring macrocycle (Fig. 4b). The $H_2TPyzPz^{\bullet-}$ radical anions of the second type are completely isolated by bulky cryptand[2.2.2][K^+] cations and solvent molecules, and there are no short vdW contacts between them.

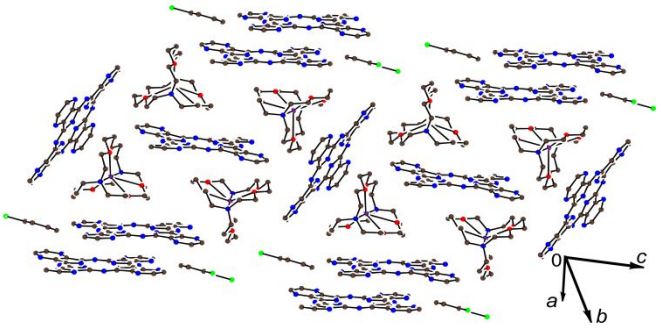

Figure 3. Crystal structure of **1**. Hydrogen atoms are not shown.

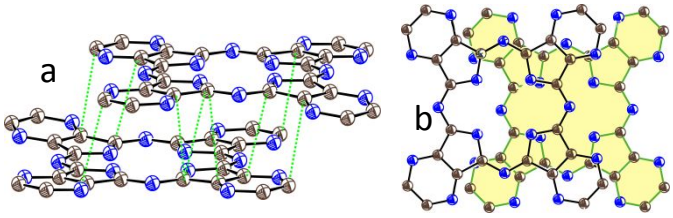

Figure 4. Dimer formed by the $H_2TPyzPz^{\bullet-}$ radical anions in **1.** Hydrogen atoms are not shown: (a) side view (short C,N…C,N contacts are shown by green dashed lines); (b) overlapping mode for two $H_2TPyzPz^{\bullet-}$ in the dimer. The macrocycle at the bottom is shown by yellow color and green bonds.

Salts **2** and **3** have structures with isolated $H_2TPyzPz^{2-}$ dianions due to the absence of vdW C, N···C,N contacts between them (Fig. 5).

These macrocycles are separated by the cryptand[2.2.2.][K^+] cations and *o*-dichlorobenzene molecules in **2**. In salt **3** there are two types of macrocycles. The first type macrocycles are surrounded by cryptand[2.2.2][K^+] cations and the $[CpFe(CO)_2]_2$ dimers which form rather short hydrogen bonds between hydrogen atoms of Cp ligand and imine and pyrazine nitrogen atoms of $H_2TPyzPz^{2-}$. Totally four such bonds are formed with the length of the H(Cp)···N($H_2TPyzPz^{2-}$) contacts in the 2.37-2.69 Å range. At the same time the shortest N_{meso}, $N_{pyrazine}$ – Fe($[CpFe(CO)_2]_2$) distances are only 4.603 Å. The second type dianions show close contacts with cryptand[2.2.2.](K^+) and solvent *o*-dichlorobenzene molecules.

The relative position of solvent molecules to the macrocycles is the same to that for $[CpFe(CO)_2]_2$ dimers to the macrocycle of first type. However, due to severe disorder these solvent molecules as well as other solvent $C_6H_4Cl_2$ molecules were squeezed by standard Olex2 routine (totally six solvent molecules per unit cell).

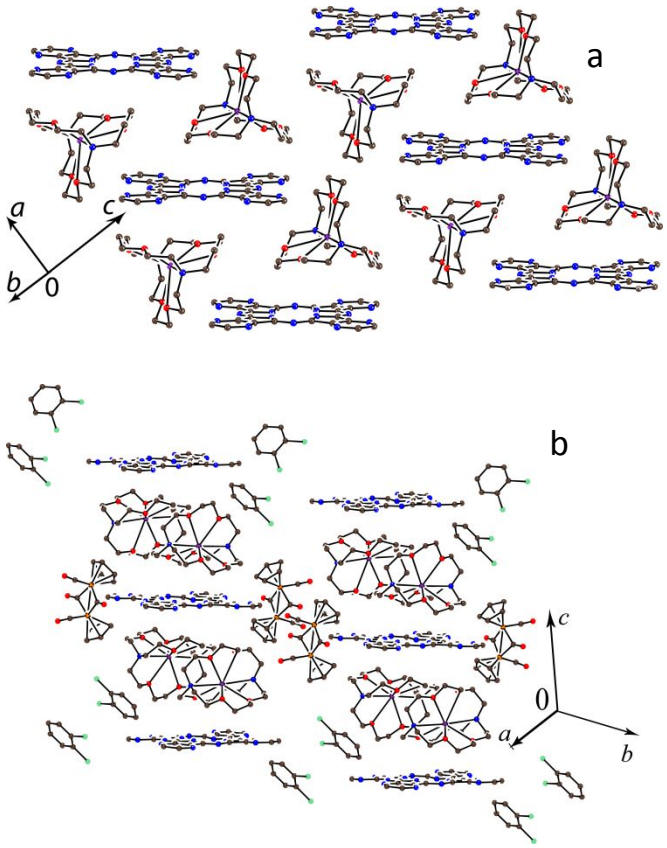

Figure 5. Crystal structures of salts **2** (a) and **3** (b). Hydrogen atoms are not shown. Solvent $C_6H_4Cl_2$ molecules are omitted for clarity

Magnetic properties

Magnetic properties of **1**-**3** were studied by EPR and for **1** by SQUID techniques on polycrystalline samples sealed in anaerobic conditions. Effective magnetic moment of salt **1** is 1.69 μ_B at 300 K (Fig. 6b) that is close to the value of 1.73 μ_B calculated for a system with one noninteracting S = 1/2 spin. The origin of spin is assigned to the $H_2TPyzPz^{\bullet-}$ radical anions. The observed temperature dependence of molar magnetic susceptibility (Fig. 6a) is well fitted as the sum of two nearly equal contributions. One contribution (about 50 % of spins) shows paramagnetic behavior with Weiss temperature of only – 1.2 K indicating very weak antiferromagnetic coupling of spins (Fig. 6a). In the crystal structure of **1**, the half numbers of $H_2TPyzPz^{\bullet-}$ is completely isolated from the neighbors and therefore paramagnetic contribution can be attributed to these species. The second contribution of about 50% of spins has essentially larger negative Weiss temperature (which however cannot be determined correctly due to too small linear high-temperature region on the temperature dependence of reciprocal molar magnetic susceptibility). Since another 50% of $H_2TPyzPz^{\bullet-}$ are packed in the dimers with effective π-π interaction between them, the second contribution can be attributed to the π-stacking dimers. This contribution can be obtained after the subtraction of another paramagnetic species contribution from the experimental data (Fig. 6c). Contribution from the dimers can be well approximated by the Heisenberg model for isolated pairs of antiferromagnetically interacting spins [41] with J/k_B = -140 K (red curve in Fig. 6c). The magnitude of exchange interactions indicates that very effective magnetic coupling of spins is realized in the π-stacking dimers. As a result, the contribution from the dimers attains maximum at about 170 K and decreases strongly below 140 K due to antiparallel arrangement of spins within the dimers. Previously it was shown that in some cases effective magnetic coupling of spins can attain J/k_B = -254 K when the π-stacking dimers show short interplanar distances and no essential shift relative to each other 22]. As a result, strong magnetic coupling of spins in the dimers suppresses their contribution in comparison with the contribution from isolated paramagnetic $H_2TPyzPz^{\bullet-}$ nearly in the whole studied temperature range. That is also the reason why the magnetic moment of **1** was slightly lower than that expected for free spins at 300 K.

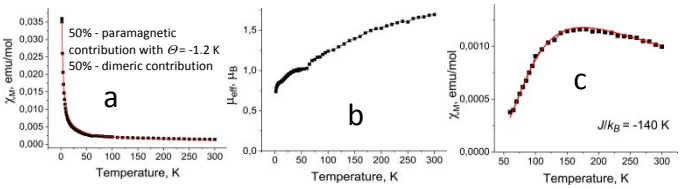

Figure 6. Temperature dependence of: (a) molar magnetic susceptibility (experimental data are black squares and the fitting is shown by red curve, see text) and (b) effective magnetic moment of polycrystalline salt **1**. (c) Molar magnetic susceptibility originated from the dimer obtained by subtracting paramagnetic contibution (C = 0.185, Θ = -1.2) from the experimental data. Fitting was made by the Heisenberg model for isolated pairs of antiferromagnetically interacting spins[19] with J/k_B = -140 K (red curve).

The EPR spectrum of polycrystalline salt **1** (Fig. 7) contains an intense asymmetric relatively narrow signal which can be fitted well by the sum of three lines with g–factors close to free-electron value (g_1 = 2.0025 and the linewidth ΔH = 0.59 mT, g_2 = 2.0061 and ΔH = 0.52 mT, g_3 = 2.0041 and ΔH = 0.44 mT) at room temperature (RT) (Fig. 7b). The g-factors and ΔH values of the lines remain almost unchanged down to 4 K (Fig. 7a, Fig. S2). A similar EPR signal is also characteristic of free-base $H_2Pc^{\bullet-}$ radical anions [19]. Again in EPR the contribution from isolated paramagnetic $H_2TPyzPz^{\bullet-}$ species dominates the spectra.

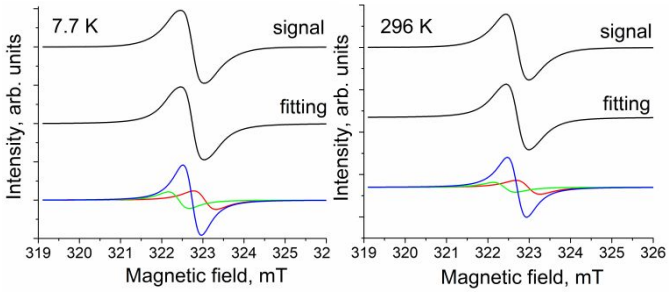

Figure 7. EPR spectra of polycrystalline **1** at 7.7 and 296 K.

It is known that the $H_2TPyzPz^{2-}$ dianions are diamagnetic and EPR silent according to previous research for salt **4** [31]. $[CpFe(CO)_2]_2$ is also EPR silent in salt **3**. EPR measurements of salts **2** and **3** supported the formation of diamagnetic $H_2TPyzPz^{2-}$ dianions. The EPR spectra of salts **2** and **3** in the 4.2 - 300 K range contain a weak asymmetric signal which can be simulated well by three narrow components with *g*–factor value close to free-electron value (Figs. S3, S4). Integral intensity of these signals is very low (less than 1% of spins from total amount of tetrapyrazinoporphyrazine) and these signals can be attributed to paramagnetic impurities. It is seen that parameters of the signals observed in **2** and **3** are very close to those attributed to $H_2TPyzPz^{\bullet-}$ in **1**. Therefore, impurity signals can be attributed to small amount of $H_2TPyzPz^{\bullet-}$ appeared in the sample due to oxidation of very air-sensitive $H_2TPyzPz^{2-}$ dianions.

Conclusions

Crystalline radical anion $\{cryptand[2.2.2](K^+)\}_2(H_2TPyzPz^{\bullet-})_2{\cdot}3C_6H_4Cl_2$ (**1**) and dianion salts $\{cryptand[2.2.2](K^+)\}_2(H_2TPyzPz^{2-}){\cdot}C_6H_4Cl_2$ (**2**) and $\{cryptand[2.2.2](K^+)\}_2$ $(H_2TPyzPz^{2-}){\cdot}[CpFe(CO)_2]_2{\cdot}3C_6H_4Cl_2$ (**3**) were obtained by the reduction of free-base tetrapyrazinoporphyrazine in the selected experimental conditions followed by precipitation of crystals by *n*-hexane. It was shown that the increase of negative charge on tetrapyrazinoporphyrazine macrocycle is accompanied by blue shift of the Soret and Q-bands (this shift is essentially larger for the dianions in comparison with the radical anions). Alternation of the $C\text{-}N_{meso}$ bonds is observed at the reduction of $H_2TPyzPz$ and is also essentially larger for $H_2TPyzPz^{2-}$ than for $H_2TPyzPz^{\bullet-}$. Salt **1** contains paramagnetic $H_2TPyzPz^{\bullet-}$ radical anions in two forms. Along with the isolated ones with negligible magnitude of magnetic coupling, the face-to-face π-stacking dimers with strong magnetic coupling of spins (J/k_B = -140 K) can also be obtained. The $H_2TPyzPz^{2-}$ dianions are diamagnetic in **2** and **3**. Among porphyrins, phthalocyanine and naphthalocyanine tetrapyrazinoporphyrazine macrocycles have strongest acceptor properties. Tetrapyrazinoporphyrazine manifests similar optical, magnetic and structural properties at the reduction to the mono- and the dianion state as other free-base macrocycles studied previously. Tetrapyrazinoporphyrazine has more stable mono- and dianions, and therefore, more air-stable functional anionic compounds can be obtained based on them.

Experimental

Materials

Diazabicyclo[8.8.8]hexacosane (cryptand[2.2.2], TCI chemicals, 98%), vanadocene (Strem, 98%), cyclopentadienyliron dicarbonyl dimer ($[CpFe(CO)_2]_2$, Sigma Aldrich, 99 %), and potassium graphite (KC_8, Strem) were used as received. Free-base tetrapyrazinoporphyrazine ($H_2TPyzPz$) was obtained as described [31]. Solvents were purified in argon atmosphere. *o*-dichlorobenzene ($C_6H_4Cl_2$) was distilled over CaH_2 under reduced pressure and *n*-hexane was distilled over Na/benzophenone. The solvents were degassed and stored in a glove box with controlled inert atmosphere (H_2O < 1 ppm, O_2 < 1 ppm) of argon. The crystals of **1-3** were stored in a glove box. KBr pellets for IR- and UV-visible-NIR measurements were also prepared in a glove box. EPR and SQUID measurements were performed on polycrystalline samples of **1-3** sealed in 2 mm quarz tubes under ambient pressure of argon.

Syntheses of crystalline salts 1-3

All the following manipulations were made in a globe box. Crystals of **1-3** were obtained by diffusion technique. The reaction solution was filtered in a 50 mL glass tube of 1.8 cm diameter with a ground glass plug, and 30 mL of *n*-hexane was layered over the solution. Slow mixing of two solvents during 1 month provided precipitation of crystals on the walls of the tube. The solvent was decanted from the crystals and they were washed with *n*-hexane.

Salt $\{cryptand[2.2.2](K^+)\}_2(H_2TPyzPz^{\bullet-})_2{\cdot}3C_6H_4Cl_2$ (**1**) was obtained by reduction of 21.9 mg of $H_2TPyzPz$ (0.042 mmol) by an excess of potassium graphite (20.0 mg, 0.148 mmol) in the presence of one equivalent of cryptand[2.2.2.] (16 mg, 0.042 mmol) by stirring overnight at 80°C till complete dissolution of $H_2TPyzPz$ and the formation of deep blue solution. Final solution was cooled down to room temperature and filtered into a tube for diffusion. Crystals in form of metallic dark black block were obtained in 63% yield.

For the synthesis of salt $\{cryptand[2.2.2](K^+)\}_2(H_2TPyzPz^{2-}){\cdot}C_6H_4Cl_2$ (**2)** solution containing $\{cryptand[2.2.2](K^+)\}(H_2TPyzPz^{\bullet-})$ was generated in *o*-dichlorobenzene. After that the solution was filtered into the flask containing about two equivalents of vanadocene (16 mg, 0.086 mmol), and solution was additionally stirred overnight at 80°C to turn deep-violet. The final solution was cooled down and filtered into a tube for diffusion. Crystals in form of metallic dark black needles were obtained in 43% yield.

Salt $\{cryptand[2.2.2](K^+)\}_2(H_2TPyzPz^{2-}){\cdot}$ $[CpFe(CO)_2]_2{\cdot}3C_6H_4Cl_2$ (**3**) was obtained by reduction of 21.9 mg of $H_2TPyzPz$ (0.042 mmol) by an excess of potassium graphite (20 mg, 0.148 mmol) in the presence of two equivalents of cryptand[2.2.2.] (32 mg, 0.084 mmol) and an excess of $[CpFe(CO)_2]_2$ (36 mg, 0.104 mmol) by stirring overnight at 80°C till complete dissolution of $H_2TPyzPz$ and the formation of deep-violet solution. Final solution was cooled down and filtered into a tube for diffusion. Crystals in form of metallic dark black blocks were obtained in 68% yield.

The compositions of **1-3** were determined from X-ray diffraction on single crystals. The analysis of obtained crystals under microscope in a glove box as well as testing of several single crystals from one synthesis by X-ray diffraction showed that only one crystalline phase formed. Elemental analysis cannot be used to confirm the composition of the crystals due to their air sensitivity and the addition of oxygen during the procedure of elemental analysis.

General

UV-visible-NIR spectra were measured in KBr pellets on a PerkinElmer Lambda 1050 spectrometer in the 250-2500 nm range. FT-IR spectra were obtained in KBr pellets with a PerkinElmer Spectrum 400 spectrometer (400-7800 cm^{-1}). EPR spectra were recorded on polycrystalline samples of **1-3** from 4.1 up to 295 K with a JEOL JES-TE 200 X-band ESR spectrometer equipped with a JEOL ES-CT470 cryostat. A Quantum Design MPMS-XL SQUID magnetometer was used to measure static magnetic susceptibility of **1** at 100 mT magnetic field in cooling and heating conditions in

the 300 - 1.9 K range. A sample holder contribution and core temperature independent diamagnetic susceptibility (χ_d) were subtracted from the experimental values. The χ_d values for salt **1** were obtained by the extrapolation of the data (170-300 K) in the high-temperature range by fitting the data with the following expression: $\chi_M = C/(T - \Theta) + \chi_d$, where C is Curie constant and Θ is Weiss temperature. Effective magnetic moment (μ_{eff}) was calculated with formula: $\mu_{eff} = (8 \cdot \chi_M \cdot T)^{1/2}$.

X-ray crystal structure determination

The data (Table 3) were collected on an Oxford diffraction "Gemini-R" CCD diffractometer with graphite monochromated MoK_α radiation using an Oxford Instrument Cryojet system. Raw data reduction to F^2 was carried out using CrysAlisPro, Oxford Diffraction Ltd. The structures were solved by direct method and refined by the full-matrix least-squares method against F^2 using SHELX 2016 [42] and Olex2 [43]. Non-hydrogen atoms were refined in the anisotropic approximation. Positions of hydrogen atoms were calculated geometrically.

Table 3. X-ray diffraction data for **1-3**.

Compound	**1**	**2**	**3**
Emp. Formula	$C_{102}H_{104}Cl_6K_2N_{36}O_{12}$	$C_{66}H_{86}Cl_2K_2N_{20}O_{12}$	$C_{92}H_{104}Cl_6Fe_2K_2N_{20}O_{16}$
M_r [g·mol^{-1}]	2317.11	1500.64	2148.55
Color and shape	metallic dark black block	metallic dark black needle	metallic dark black block
Crystal system	triclinic	triclinic	triclinic
Space group	$P\bar{1}$	$P\bar{1}$	$P\bar{1}$
a, Å	13.7277(3)	9.8535(3)	13.2775(3)
b, Å	19.2901(5)	15.7516(7)	18.5439(5)
c, Å	23.1243(6)	24.2437(11)	23.0154(5)
α, °	66.352(2)	102.290(4)	108.314(2)
β, °	74.863(2)	99.291(3)	94.677(2)
γ, °	89.576(2)	95.730(3)	110.394(2)
V, Å^3	5381.8(2)	3593.0(3)	4925.0(2)
Z	2	2	2
ρ_{calc} [g/cm^3]	1.430	1.387	1.449
μ [mm^{-1}]	0.316	0.281	0.543
F(000)	2408	1580	2224
T [K]	113(2)	112(2)	115(6)
Max. 2Θ , °	59.372	59.334	59.438
Reflns measured	70854	34558	55588
Unique reflns	25903	16824	23542
Parameters	1484	919	1102
Restraints	192	0	498
Reflns[F_o>2(F_o)]	19105	8843	18062
R_1 [F_o>2σ(F_o)]	0.0627	0.0677	0.0485
WR_2 (all data)[a],	0.1731	0.1378	0.1276
G.O.F	1.013	1.031	1.013
CCDC number	1952192	1952193	1952194

The structure of **1** contains one disordered $C_6H_4Cl_2$ molecule with 0.636(2)/0.364(2) occupancies. The structure of **3** also contains a disordered part of one cryptand[2.2.2.](K^+) molecule with 0.737(6)/0.263(6) occupancies as well as cyclopentadienyl (Cp) ligands of $\{CpFe(CO)_2\}_2$ are disordered with 0.600(11)/0.400(11) and 0.753(15)/0.247(15) occupancies. In the structure of **3** there are six strongly disordered *o*-dichlorobenzene molecules per unit cell which were squeezed by standard Olex2 routine.

Conflicts of interest

There are no conflicts to declare.

Acknowledgements

The work was supported by Russian Science Foundation (project № 19-73-00287) and the Kyoto University Foundation, and the JST (ACCEL) 27 (100150500019) project.

Notes and references

1 *Phthalocyanines: Properties and Applications* (Eds.: C. C. Leznoff, A. B. P. Lever), Wiley-VCH, Cambridge, 1989-1996, Vols. 1 – 4.
2 Handbook of Porphyrin Science: with Applications to Chemistry, Physics, Materials Science, Engineering, Biology and Medicine (Eds.: K. M. Kadish, M. Smith, R. Guilard), World Scientific, 2010, Vol. 1.
3 M. G. Walter, A. B. Rudine and C. C. Wamser, *J. Porphyrins Phthalocyanines*, 2010, **14**, 759–792. 10.1142/S1088424610002689
4 D. Wöhrle, G. Schnurpfeil, S. G. Makarov, A. Kazarin and O. N. Suvorova, *MHC*, 2012, **5**, 191–202. 10.6060/mhc2012.120990w
5 O. L. Kaliya, E. A. Lukyanets and G. N. Vorozhtsov, *J. Porph. Phth.*, **1999**, 3, 592 – 610. https://doi.org/10.1002/(SICI)1099-1409(199908/10)3:6/7<592::AID-JPP180>3.0.CO;2-G
6 T. Inabe and H. Tajima, *Chem. Rev.*, 2004, **104**, 5503–5534. 10.1021/cr030649x
7 H. Hasegawa, T. Naito, T. Inabe, T. Akutagawa and T. Nakamura, *J. Mater. Chem.*, 1998, **8**, 1567–1570. 10.1039/a800123e
8 J. S. Miller, C. Vazquez, J. C. Calabrese, R. S. McLean and A. J. Epstein, *Adv. Mater.*, 1994, **6**, 217–221. 10.1002/adma.19940060306
9 D. K. Rittenberg, L. Baars-Hibbe, A. Böhm and J. S. Miller, *J. Mater. Chem.*, 2000, **10**, 241–244. 10.1039/A907159H
10 E. Tosatti, M. Fabrizio, J. Tóbik and G. E. Santoro, *Phys. Rev. Lett.*, 2004, **93**, 117002. 10.1103/PhysRevLett.93.117002
11 D. V. Konarev, L. V. Zorina, S. S. Khasanov, E. U. Hakimova and R. N. Lyubovskaya, *New J. Chem.*, 2012, **36**, 48–51. 10.1039/C1NJ20858F
12 D. V. Konarev, M. Ishikawa, S. S. Khasanov, A. Otsuka, H. Yamochi, G. Saito and R. N. Lyubovskaya, *Inorg. Chem.*, 2013, **52**, 3851–3859. 10.1021/ic3025364
13 D. V. Konarev, L. V. Zorina, M. Ishikawa, S. S. Khasanov, A. Otsuka, H. Yamochi, G. Saito and R. N. Lyubovskaya, *Crystal Growth & Design*, 2013, **13**, 4930–4939. 10.1021/cg401118s
14 J. A. Cissell, T. P. Vaid and A. L. Rheingold, *Inorg. Chem.*, 2006, **45**, 2367–2369. 10.1021/ic051794r

15 E. W. Y. Wong and D. B. Leznoff, *J. Porphyrins Phthalocyanines*, 2012, **16**, 154–162. 10.1142/S1088424611004440

16 E. W. Y. Wong, C. J. Walsby, T. Storr and D. B. Leznoff, *Inorg. Chem.*, 2010, **49**, 3343–3350. 10.1021/ic902409n

17 W. Zhou, R. H. Platel, T. Teixeira Tasso, T. Furuyama, N. Kobayashi and D. B. Leznoff, *Dalton Trans.*, 2015, **44**, 13955–13961. 10.1039/c5dt01778e

18 D. V. Konarev, S. S. Khasanov, M. Ishikawa, A. Otsuka, H. Yamochi, G. Saito and R. N. Lyubovskaya, *Dalton Trans.*, 2017, **46**, 3492–3499. 10.1039/c7dt00336f

19 D. V. Konarev, A. V. Kuzmin, M. A. Faraonov, M. Ishikawa, S. S. Khasanov, Y. Nakano, A. Otsuka, H. Yamochi, G. Saito and R. N. Lyubovskaya, *Chem. Eur. J.*, 2015, **21**, 1014–1028. 10.1002/chem.201404925

20 D. V. Konarev, M. A. Faraonov, A. V. Kuzmin, S. S. Khasanov, Y. Nakano, S. I. Norko, M. S. Batov, A. Otsuka, H. Yamochi, G. Saito and R. N. Lyubovskaya, *New J. Chem.*, 2017, **41**, 6866–6874. 10.1039/c7nj00530j

21 D. V. Konarev, S. I. Troyanov, A. V. Kuzmin, Y. Nakano, M. Ishikawa, M. A. Faraonov, S. S. Khasanov, A. L. Litvinov, A. Otsuka, H. Yamochi, G. Saito and R. N. Lyubovskaya, *Inorg. Chem.*, 2017, **56**, 1804–1813. 10.1021/acs.inorgchem.6b01932

22 D. V. Konarev, A. V. Kuzmin, S. S. Khasanov, M. S. Batov, A. Otsuka, H. Yamochi, H. Kitagawa and R. N. Lyubovskaya, *CrystEngComm*, 2018, **20**, 385–401. 10.1039/c7ce01918a

23 D. V. Konarev, A. V. Kuzmin, S. S. Khasanov, A. L. Litvinov, A. Otsuka, H. Yamochi, H. Kitagawa and R. N. Lyubovskaya, *Chem. Asian J.*, 2018, **13**, 1552–1560. 10.1002/asia.201701754

24 D. V. Konarev, Y. Nakano, S. S. Khasanov, A. V. Kuzmin, M. Ishikawa, A. Otsuka, H. Yamochi, G. Saito and R. N. Lyubovskaya, *Crystal Growth & Design*, 2017, **17**, 753–762. 10.1021/acs.cgd.6b01612

25 D. V. Konarev, A. V. Kuzmin, M. Ishikawa, Y. Nakano, M. A. Faraonov, S. S. Khasanov, A. Otsuka, H. Yamochi, G. Saito and R. N. Lyubovskaya, *Eur. J. Inorg. Chem.*, 2014, **2014**, 3863–3870. 10.1002/ejic.201400126

26 D. V. Konarev, S. S. Khasanov, M. S. Batov, A. G. Martynov, I. V. Nefedova, Y. G. Gorbunova, A. Otsuka, H. Yamochi, H. Kitagawa and R. N. Lyubovskaya, *Inorg. Chem.*, 2019, **58**, 5058–5068. 10.1021/acs.inorgchem.9b00131

27 K. Takahashi, Y. Aoki, T. Sugitani, F. Moriyama, Y. Tomita, M. Handa, K. Kasuga and K. Sogabe, *Inorganica Chimica Acta*, 1992, **201**, 247–249. 10.1016/S0020-1693(00)85340-2

28 K. Ohta, T. Watanabe, T. Fujimoto and I. Yamamoto, *J. Chem. Soc., Chem. Commun.*, 1989, 1611. 10.1039/C39890001611

29 A. B. P. Lever, E. R. Milaeva, G. Speier in Phthalocyanines: Properties and Applications, Vol. 3 (Eds.: C. C. Leznoff, A. B. P. Lever), VCH Publishers, New York, 1993, pp. 1 – 69.

30 V. Novakova, M. P. Donzello, C. Ercolani, P. Zimcik and P. A. Stuzhin, *Coordination Chemistry Reviews*, 2018, **361**, 1–73. 10.1016/j.ccr.2018.01.015

31 D. V. Konarev, M. A. Faraonov, A. V. Kuzmin, A. M. Fatalov, N. G. Osipov, S. S. Khasanov, A. F. Shestakov and R. N. Lyubovskaya, *ChemistrySelect*, 2018, **3**, 4339–4343. 10.1002/slct.201800739

32 M. A. Faraonov, D. V. Konarev, A. M. Fatalov, S. S. Khasanov, S. I. Troyanov and R. N. Lyubovskaya, *Dalton Trans.*, 2017, **46**, 3547–3555. 10.1039/c6dt04896j

33 M.A. Faraonov, N.R. Romanenko, A.V. Kuzmin, D.V. Konarev, S.S.Khasanov, R.N. Lyubovskaya, *Macroheterocycles*, in press 10.6060/mhc190451f

34 M. A. Faraonov, N. R. Romanenko, A. V. Kuzmin, D. V. Konarev, A. F. Shestakov, P. A. Stuzhin, S. S. Khasanov, A. Otsuka, H. Yamochi, H. Kitagawa and R. N. Lyubovskaya, *Eur. J. Inorg. Chem.*, 2019, **2019**, 2918–2923. 10.1002/ejic.201900511

35 R. O. Loutfy, C. K. Hsiao, B. S. Ong and B. Keoshkerian, *Can. J. Chem.*, 1984, **62**, 1877–1885. https://doi.org/10.1139/v84-322

36 P. Vaný́sek, Electrochemical series, in W. M. Haynes (Ed.). *Handbook of Chemistry and Physics: 93rd Edition*, Chemical Rubber Company, **2012**, pp. 5 – 80

37 V. Novakova, P. Reimerova, J. Svec, D. Suchan, M. Miletin, H. M. Rhoda, V. N. Nemykin and P. Zimcik, *Dalton Trans.*, 2015, **44**, 13220–13233. 10.1039/c5dt01863c

38 E. Viola, M. P. Donzello, S. Ciattini, G. Portalone and C. Ercolani, *Eur. J. Inorg. Chem.*, 2009, **2009**, 1600–1607. 10.1002/ejic.200900029

39 K. A. Ustimenko, D. V. Konarev, S. S. Khasanov and R. N. Lyubovskaya, *Macroheterocycles*, 2013, **6**, 345–352. 10.6060/mhc131162k

40 S. Matsumoto, K. Matsuhama and J. Mizuguchi, *Acta Crystallogr C Cryst Struct Commun*, 1999, **55**, 131–133. 10.1107/S0108270198011020

41 J. S. Smart, In Magnetism III; G. T. Rado, H. Suhl, Eds.; 881 Academic Press: New York, 1963; p 63

42 G. M. Sheldrick, *Acta Crystallogr A Found Crystallogr*, 2008, **64**, 112–122. 10.1107/S0108767307043930

43 O. V. Dolomanov, L. J. Bourhis, R. J. Gildea, J. A. K. Howard and H. Puschmann, *J Appl Crystallogr*, 2009, **42**, 339–341. 10.1107/S0021889808042726

ARTICLE

Article for TOC

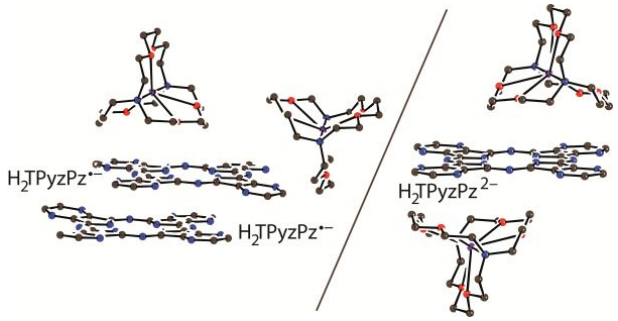

Synthesis, spectral and structural characterization of the novel radical anion and dianion salts of free-base tetrapyrazinoporphyrazine ($H_2TPyzPz$) as well as studies of their magnetic properties are described.